Title

Large-eddy simulations of flow and heat transfer in heated concentric annulus with inner cylinder rotation

Authors

Schneider, M
Younis, BA
Weigand, B

Publication Date

2017-11-01

DOI

10.1016/j.ijheatmasstransfer.2017.07.022

Peer reviewed

International Journal of Heat and Mass Transfer 114 (2017) 1248–1262

Contents lists available at ScienceDirect

International Journal of Heat and Mass Transfer

journal homepage: www.elsevier.com/locate/ijhmt

Large-eddy simulations of flow and heat transfer in heated concentric annulus with inner cylinder rotation

M. Schneider [a], B.A. Younis [b,*], B. Weigand [c]

[a] Institut für Bauweisen und Strukturtechnologie, German Aerospace Center (DLR), 70569 Stuttgart, Germany
[b] Department of Civil & Environmental Engineering, University of California, Davis, CA 95616, USA
[c] Institut für Thermodynamik der Luft- und Raumfahrt, Universität Stuttgart, 70569 Stuttgart, Germany

ARTICLE INFO

Article history:
Received 23 June 2017
Received in revised form 1 July 2017
Accepted 4 July 2017
Available online 14 July 2017

Keywords:
Destabilizing rotation
Concentric annulus
LES
Heat transfer

ABSTRACT

Results from large-eddy simulations are reported for the flow and heat transfer in the annular gap between two concentric cylinders with the outer cylinder stationary and the inner cylinder rotating about its longitudinal axis. The objective of the study was to document the effects of destabilizing rotation on the turbulent transport of heat and momentum. The inner cylinder was heated by applying a constant heat flux while the conditions at the outer wall were adiabatic. Results were obtained for a stationary inner cylinder to serve as baseline for isolating the effects of rotation, and for the inner cylinder rotated at two different rotation numbers viz. 0.21 and 0.86. The Reynolds number was set at 9000 for all cases. With the outer cylinder stationary and the inner cylinder rotating, the effects of rotation are to destabilize the turbulence leading to enhanced mixing and significant increase in wall shear stress and Nusselt number. Additional effects include the displacement from each other of the points where the Reynolds stresses and the corresponding rates of strain are zero, and the non-alignment of their respective directions. These and other results reported herein provide a useful contribution to the very limited literature on heated turbulent flows destabilized by rotation, and can serve as benchmark to aid in the development and validation of turbulence closures for engineering applications.

1. Introduction

The importance from both fundamental and practical standpoints of the study of the effects of rotation on turbulence is evidenced by the substantial body of published literature on the subject. Nowhere are these effects more immediately apparent than in the case of flows in single or concentric cylinders that are rotated about their longitudinal axis. For the case of the flow in a single rotating cylinder, the gradient of angular momentum is positive away from the axis of rotation and thus, according to Rayleigh's stability criteria [1], the effects of rotation are stabilizing leading to reduction in turbulence activity relative to the non-rotating case. Results for this flow have been obtained by utilizing all the tools that are available for the study of fluid-flow phenomena including analytical solutions [2,3], experiments [4,5], large-eddy and direct numerical simulations [6–9] and turbulence closures [10,11]. Collectively, these studies have served to document in detail the substantial modifications of the flow and heat transfer processes wrought by stabilizing rotation. In terms of bulk flow parameters, these are seen in the significant reduction in the friction factor and in Nusselt number relative to the stationary case, and at sufficiently high rotation rates, in the suppression of turbulence such that the flow comes to exhibit a laminar-like behavior.

The present work is also concerned with the study of the effects axial rotation on turbulent pipe flow but for the far less well documented case where these effects on the turbulence structure are destabilizing. This is achieved in the annular gap between two concentric cylinders where the inner cylinder is rotating while the outer cylinder is kept stationary. In this case, the angular momentum decreases with radial distance from the axis of rotation and hence a fluid element following a circular path, once displaced from equilibrium, does not encounter a force sufficient to restore it to its original path [1]. In the presence of axial flow, this configuration is sometimes referred to as the Taylor-Couette-Poiseuille flow [12]. Here, and in contrast to the flow in a single rotating cylinder, far fewer studies have been reported, especially for the case where heat transfer is present. Fenot et al. [12] present a comprehensive review of the available experimental results from which it can be seen that, in most cases, the flow was either laminar or transitional. Their review also indicated that the heat transfer characteristics depended strongly on the entrance conditions of

* Corresponding author.
E-mail address: bayounis@ucdavis.edu (B.A. Younis).

http://dx.doi.org/10.1016/j.ijheatmasstransfer.2017.07.022
0017-9310/

Nomenclature

C_s	smagorinsky coefficient
C_f	friction coefficient $\left(=\frac{\tau_w}{\frac{1}{2}\rho U_b^2}\right)$
D	pipe diameter
L	domain length
N	rotation number $(=\Omega R/U_b)$
Nu	Nusselt number $\left(=\frac{-D_h\frac{\partial\Theta}{\partial r}\vert_w}{\Theta_w-\Theta_b}\right)$
Pr	Prandtl number
$\dot{Q}$	wall heat flux
R	pipe radius
R^*	radius ratio $(=R_1/R_2)$
R_{ij}	two-point correlations coefficient
Re	Reynolds number $(=U_bD/\nu)$
Re_t	turbulence Reynolds number $(=\frac{k^2}{\nu\varepsilon})$
Ta	Taylor number
U_i	velocity vector
u_τ	friction velocity $\left(=\sqrt{\frac{\vert\tau_w\vert}{\rho}}\right)$
$\overline{u_iu_j}$	Reynolds-stress tensor
$\overline{u_it}$	turbulent heat flux

Greek symbols

δ	half height of annular gap $(=1/2(R_2-R_1))$
ε	dissipation rate
γ_g	strain rate angle
γ_τ	Reynolds shear stress angle
ν	kinematic viscosity
Ω	rotational velocity of inner cylinder (annular) or pipe wall
ρ	density
τ_{ij}	sub-grid scale correlations in momentum equations
Θ	grid resolved temperature
Θ_τ	friction temperature $\left(=\frac{-\dot{Q}_w}{\rho c_p u_\tau}\right)$

Subscripts

1	inner wall value in annular flow
2	outer wall value in annular flow
b	bulk
s	smooth
sgs	sub-grid scale
t	turbulent
w	wall

the axial flow. This poses a problem for the computation of these flows since the inlet conditions are rarely documented in the detail that is sufficient for this purpose, especially with regards to the profiles of the turbulent kinetic energy dissipation rate - a parameter which plays a critical role in determining the patterns of flow development downstream of the inlet. For the fully turbulent case, only the experiments of Becker and Kaye [13] and Kuzay and Scott [14] appear to provide data for heated annular flow with inner cylinder rotation though their focus was largely on bulk parameters such as the torque coefficients and the Nusselt number. With regards to computations, large eddy simulations were reported by Murata and Iwamoto [15] but these were confined to the relatively low Reynolds number of 1000. Chung and Sung [16] obtained results using direct numerical simulations for $Re = 8900$ and reported that the turbulent thermal statistics near the outer wall were greater than those near the inner walls - a result which they attributed to the effects of transverse curvature. Considering the degree of uncertainty inherent in both computations and experiments, the present study was undertaken with the objective of using large eddy simulations to document the principal features of the heated flow in concentric annulus with destabilizing rotation at high Reynolds number. The aim was to further improve our understanding of the physical processes involved, and to provide data suitable for the development and verification of turbulence closures suited for engineering applications.

The remainder of this paper is in four sections. The mathematical formulation and details of the computations are presented in Section 2, the problem is defined and details of the computational procedure are presented followed in Section 3 with presentation and discussion of the results. Results for pipe and annular flows both with and without rotation are presented, the latter serving to provide a baseline for isolating the effects of rotation. Concluding remarks are presented in Section 4.

Table 1
Parameters of the computational grid.

Parameter	LES present	LES/DNS [22]	LES [23]	LES [24]	LES [25]
N_θ	124	129	129	128	65
N_r	52	39	65	64	39
N_z	154	129	129	192	65
Δr^+_{min}	0.474	0.08	0.04	0.75	
Δr^+_{max}	7.95	17.6	9.4	15	
$R\Delta\theta^+$	9.58	9.06	8.7	36	
Δx^+	28.7	36.05	27.9	30	
Length	12D	10D	10D	10D	10D

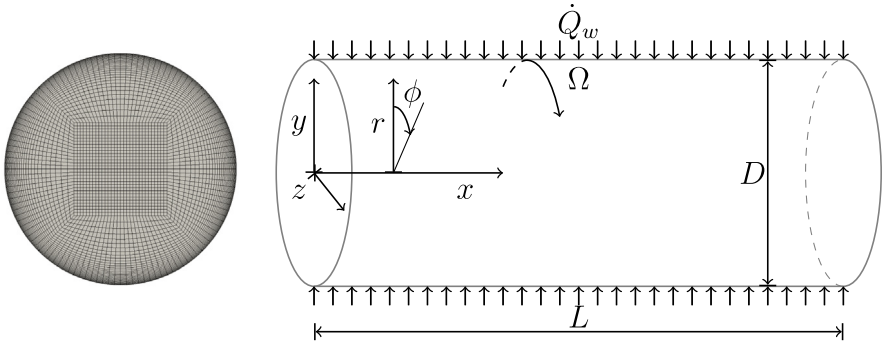

Fig. 1. Grid and schematic representation of geometry and coordinates.

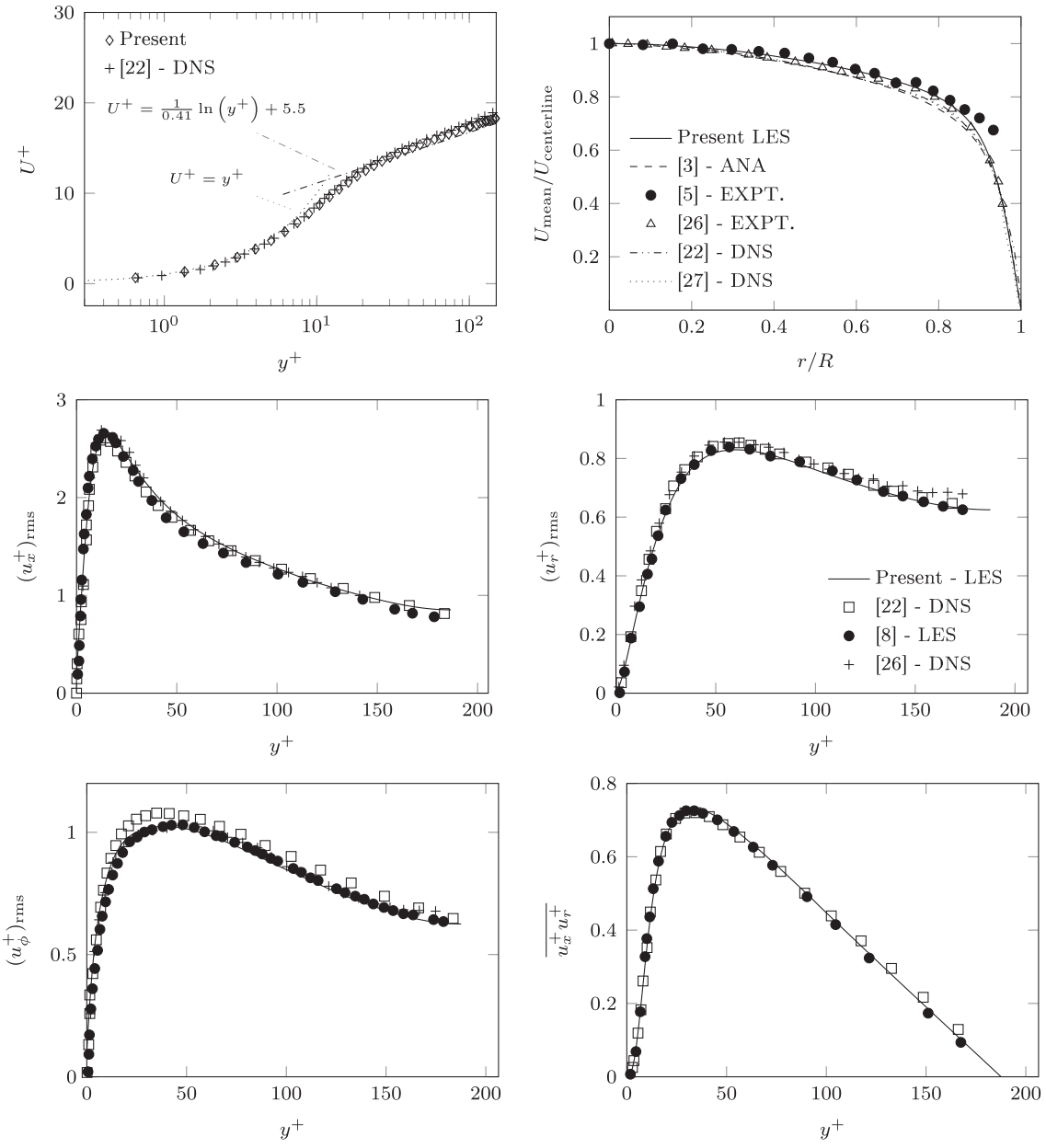

Fig. 2. Pipe flow: Mean velocity and turbulence statistics. (See above-mentioned references for further information.)

Table 2
Pipe flow: Predicted and measured Nusselt number.

	Present (Th1)	Present (Th2)	Reynolds analogy	[8] DNS	[30] DNS	[28] EXPT
Nu	18.70	19.33	19.82	19.36	18.54	18.17

2. Mathematical formulation

2.1. Governing equations

In formulating the equations that describe the flow in rotating pipes and annular gaps, a choice exists in whether these equations are cast with respect to a coordinate system that is fixed in space, or one that is rotating at the same rate as the rotating cylinder. In the former approach, body-force terms appear in the momentum equations, while in the latter approach, these terms are absent and the effects of rotation are introduced via the appropriate no-slip boundary conditions at the rotating walls. In this study, and in an effort to check the overall extent of the numerical uncertainty in the predictions, both approached were tried with results that were indistinguishable from each other. In what follows, the equations are presented with reference to a fixed coordinate system. In large eddy simulations, the equations governing the conservation of mass, momentum and thermal energy for an incompressible, constant properties fluid are expressed as:

$$\frac{\partial U_i}{\partial x_i} = 0 \tag{1}$$

$$\frac{\partial U_i}{\partial t} + U_j\frac{\partial U_i}{\partial x_j} = -\frac{1}{\rho}\frac{\partial P}{\partial x_i} + \frac{\partial}{\partial x_j}\left(\nu\frac{\partial U_i}{\partial x_j} - \tau_{ij}\right) \tag{2}$$

$$\frac{\partial \Theta}{\partial t} + U_j\frac{\partial \Theta}{\partial x_j} = \frac{\partial}{\partial x_i}\left(\Gamma\frac{\partial \Theta}{\partial x_i} - \tau_{\theta i}\right) \tag{3}$$

In the above, U_i, Θ and P are, respectively, the filtered velocity, temperature and pressure, ρ is the density, ν and Γ are the kinematic viscosity and thermal diffusivity, τ_{ij} are the turbulent correlations that represent the effects of the unresolved, sub-grid motions on the transport of momentum, and $\tau_{\theta i}$ are the corresponding terms for thermal energy [17].

Several alternative approaches to modeling the unknown turbulent correlations have been reported in the literature. For the momentum equations, the most widely used model is based on Boussinesq's hypothesis in which these correlations are made proportional to the local mean rates of strain, thus:

$$-\tau_{ij} = 2\nu_{sgs}S_{ij} \tag{4}$$

where S_{ij} is the mean rate of strain, and ν_{sgs} is a pseudo eddy viscosity:

$$S_{ij} = \frac{1}{2}\left(\frac{\partial U_i}{\partial x_j} + \frac{\partial U_j}{\partial x_i}\right) \tag{5}$$

$$\nu_{sgs} = (C_s\Delta)^2(S_{ij}S_{ij})^{0.5}\left(1 - exp\left(\frac{-y^+}{A^+}\right)\right) \tag{6}$$

In the above, Δ is the characteristic length scale taken as the cubic root of the cell volume and C_s, the Smagorinsky constant, is assigned the value of 0.065 which is widely used in the computation of wall-bounded flows. The term involving the exponential function provides for the effects of wall damping of the sub-grid scale terms. Here, y^+ is the normal distance in usual wall coordinates, and A^+ is a constant assigned its usual value of 26.

To check the sensitivity of the computed results to the sub-grid scale model, computations were performed in which the Smagorinsky constant was set equal to zero, and further computations that used Germano et al.'s [18] dynamic sub-grid scale model which, in essence, provides for Smagorinsky's constant to vary in space and in time by making it a function of Δ and S_{ij}. The results of these tests are included in Appendix A.

Modeling the sub-grid scale correlations in the thermal energy equation follows the usual approach of adopting Fourier's law to relate these correlations to the local gradients of temperature:

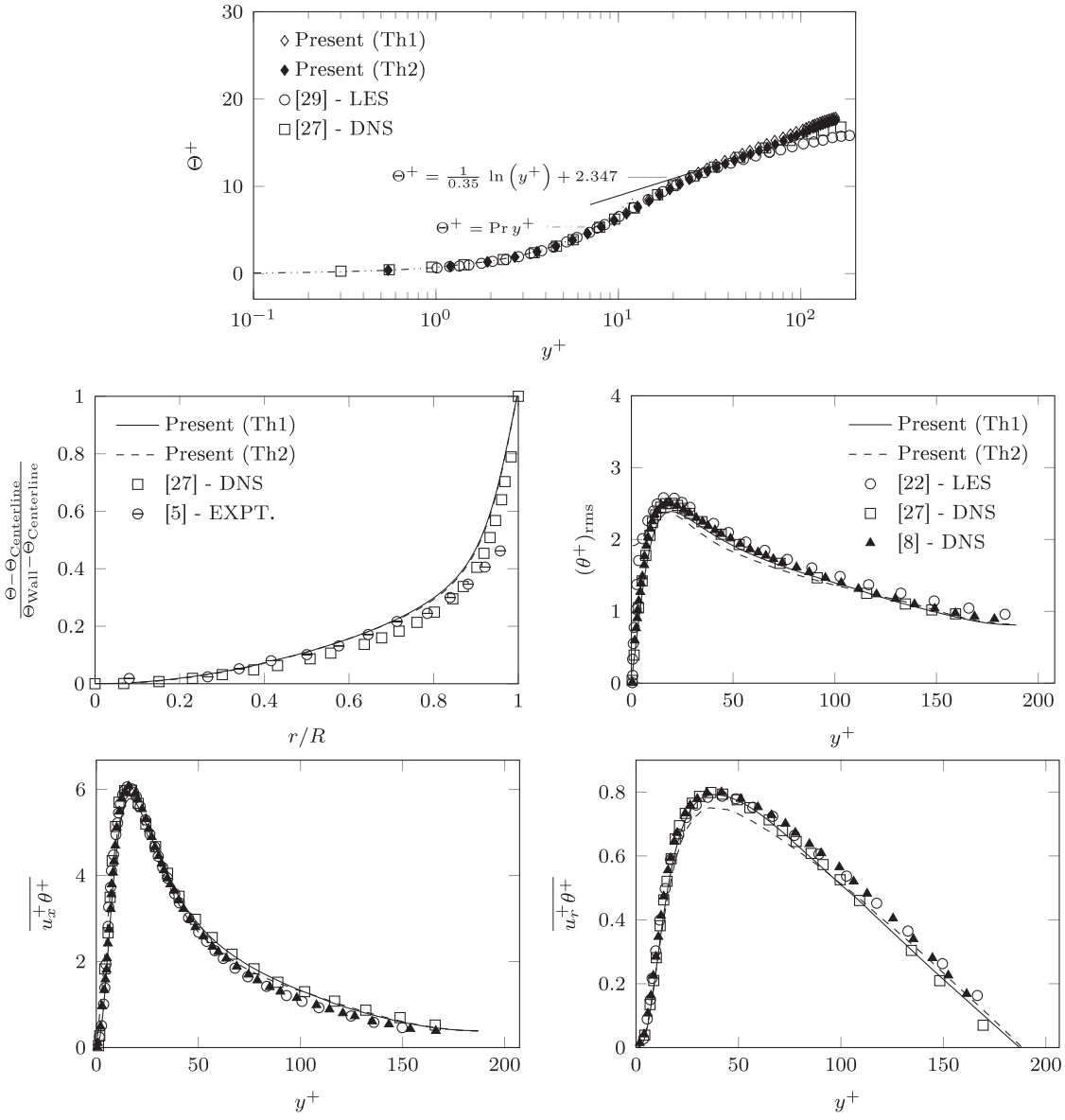

Fig. 3. Pipe flow: Predicted and measured thermal statistics. (See above-mentioned references for further information.)

$$-\tau_{\theta i} = \Gamma_{sgs}\frac{\partial \Theta}{\partial x_i}, \qquad \Gamma_{sgs} = \frac{\nu_{sgs}}{Pr_{sgs}} \tag{7}$$

In the above, Γ_{sgs} is the sub-scale thermal diffusivity, and Pr_{sgs} is the sub-grid Prandtl number assigned here the value of 0.41.

2.2. Computational details

The governing equations and associated sub-grid models were solved using the open source CFD toolbox OpenFOAM [19]. Discretization of the spatial and temporal gradients was achieved using second-order accurate schemes. In constructing the computational grids, care was taken to ensure that the flow in the near-wall region was adequately resolved as this is essential for the accurate computation of wall friction and Nusselt numbers. In all subsequent computations, the grid nodes closest to the walls were located such that the normal distance from their centers to the wall satisfied the constraint $y^+ < 1.0$. Thereafter, the grid was stretched in the radial direction constrained by an expansion ratio of 5%. The time-step size was constrained by the requirement that the Courant number remained below 0.6 everywhere in the flow-field, and at all times.

In deciding on the axial extent of the solution domain, consideration was given to two requirements: the need to obtain results that are independent of assumed inlet conditions (equivalent to obtaining measurements in the fully-developed regime), and the need to keep the computational demands within realistic bounds in order to improve the prospects of achieving an acceptable level of numerical accuracy. In this work, these requirements were met by employing cyclic boundary conditions such that the computed results at the outlet plane were successively mapped back onto the inlet plane until no further changes were detected within reasonable limits. To ensure that the longitudinal extent of the computational domain was sufficient for the large-scale turbulent

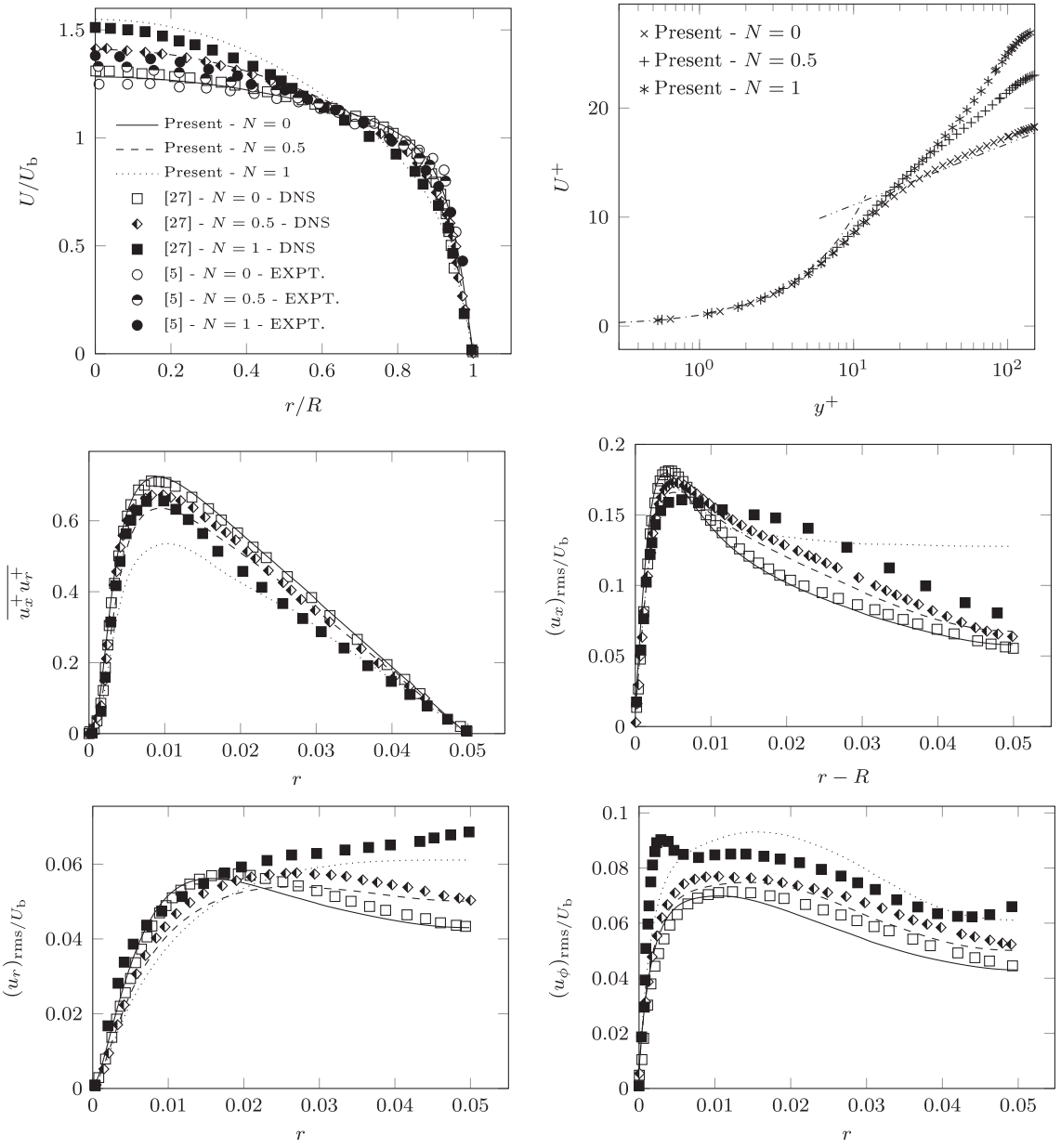

Fig. 4. Rotating pipe: Mean velocity and turbulence statistics.

motions to develop unconstrained by the boundary conditions, the computations were repeated over progressively longer domain lengths until the two-point correlations for the velocity fluctuations in all three directions dropped to effectively zero over a significant length of the domain. This was taken to indicate that the computed flow details there were effectively independent of the conditions at the boundaries. A sample of these results is presented in the next section. In implementing the cyclic boundary conditions, care was taken to ensure that the sectional-averaged velocity and the sectional-averaged modified temperature (according to Eq. 8) remained constant along the entire length of the pipe. For the velocity field, this was achieved by implementing the proposals of Patankar et al. [20] in which the pressure field is decomposed into a periodic part, and a part that provides for a constant global pressure gradient. Substitution into Eq. (2) produces a term that is linear in the axial distance (x) and whose slope represents the global pressure gradient. This slope is adjusted iteratively within the solution cycle until the desired flow rate is achieved. For the thermal field, the way in which the sectional-averaged temperature was kept constant was by recognizing that, when a uniform heat flux is applied, the bulk temperature increases linearly with axial distance (x). Thus the temperature field (Θ) can be decomposed into a periodic part, and another that takes into account the overall increase in temperature:

$$\Theta(x,y,z) = \overline{\Theta}(x,y,z) + \gamma x \tag{8}$$

The temperature gradient (γ) can be derived from consideration of the energy balance applied across the entire pipe length where it can be shown:

$$\gamma = \frac{\Theta(0,y,z) - \Theta(L,y,z)}{L} = \frac{\dot{Q}}{\dot{m} c_p L} \tag{9}$$

where $\dot{Q}$ is the heat flux into the domain, c_p is the specific heat at constant pressure and $\dot{m}$ is the mass flow rate. Substitution into Eq. (3) yields the appropriate equation for cyclic boundary conditions.

Concerning the boundary conditions at the walls, for the stationary pipe, the no-slip conditions were applied to the velocity components in all three coordinate directions. For the rotating

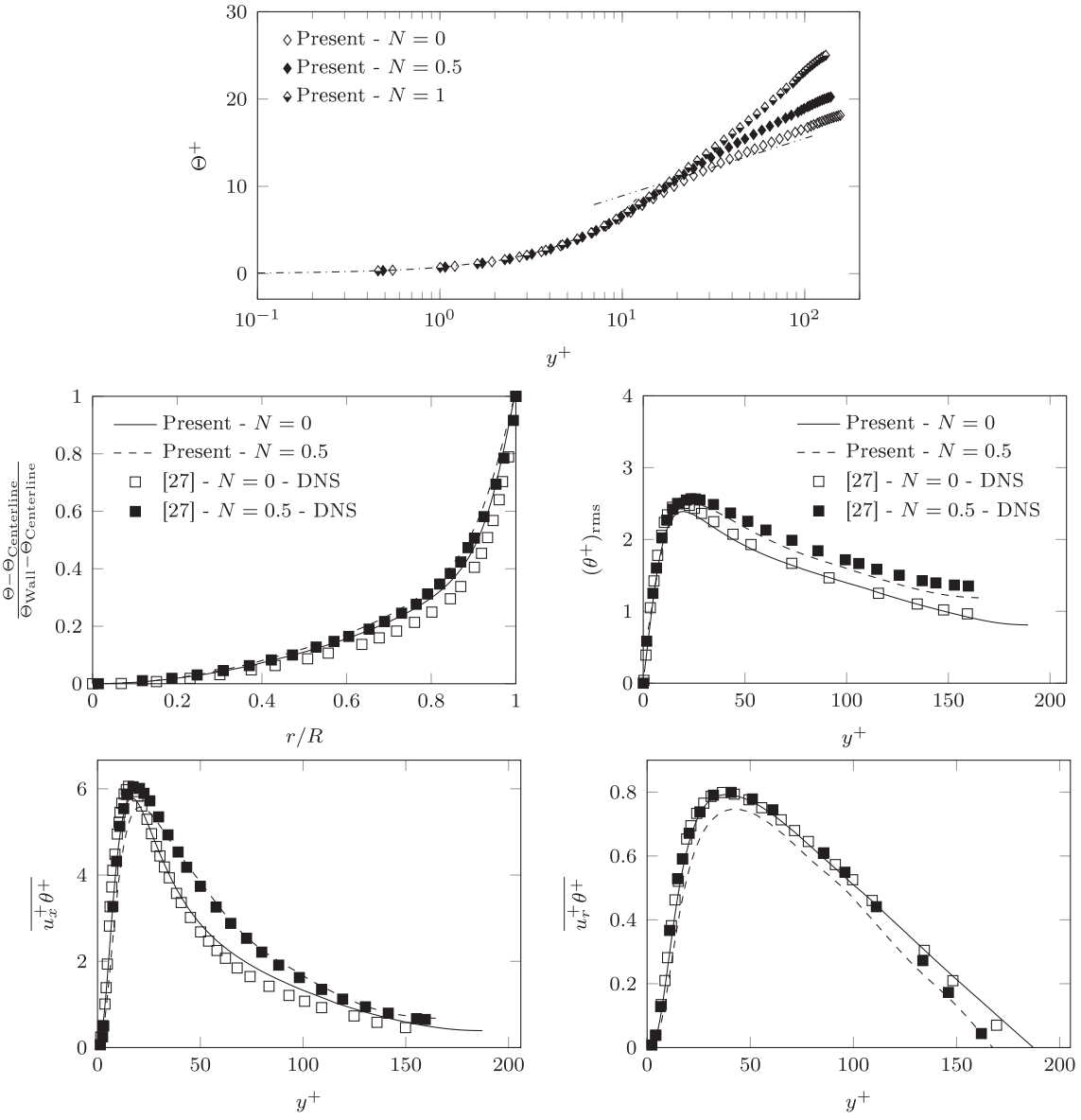

Fig. 5. Rotating pipe: Mean temperature and thermal statistics.

pipe, the velocity component in the circumferential direction was assigned a value (Ω) that yields the desired Rotation number (N):

$$N = \frac{\Omega R}{U_b} \tag{10}$$

where R is the radius of the rotating cylinder.

In performing large eddy simulations, several options for specifying the initial conditions exist, most aiming to accelerate transition to turbulence and thus aid in the establishment of a sustainable turbulence field within a reasonable time interval. A number of these options were tested in this study, and the one found to be most successful was provided by the software tool (*perturbU*), developed by De Villiers [21] and already implemented in OpenFOAM. This tool is based on the assumption that the vortical structures near the walls are essential for the initiation of turbulence via instabilities produced by the ejection of low speed flow away from the wall. To develop these structures, a laminar profile is prescribed, superimposed with random streaks. The result is a near-wall vorticity field that is of sufficient strength to be sustainable in the initial period of flow development but whose influence recede with time.

3. Results and discussion

3.1. Pipe flow

To provide basis for later analysis, results were obtained for the fully developed flow in a pipe with and without rotation. The computations were performed on a Cartesian grid, and the results transformed to cylindrical-polar coordinates for comparison with experiments. The computational grid, the cross section of which is shown in Fig. 1, was formed in five parts: a square section in the middle surrounded by four semi-circular sections. The grid spacings in all three coordinate directions were specified in accordance with the best practices of previous studies with LES and DNS as can be seen in Table 1.

Table 3
Grid resolutions for annular flow calculations.

	Present LES	[32] LES	[33] LES	[34] DNS	[35] DNS
N_x	120	120	128	128	256
N_θ	360	360	65	192	256
N_r	64	64	64	65	65
L_z	18δ	18δ	18δ	18δ	18δ
Δr^+_{in}	0.31	0.8	0.27	0.13	
Δr^+_{out}	0.27	0.7	0.23	0.12	
Δr^+_{max}	21.4		13.86	12.96	12.89
$R_{in}\Delta\theta^+$	5.7	7.1	8.01	3.75	1.84
$R_{out}\Delta\theta^+$	10.4	12.5	13.86	7.1	3.68
Δx^+	24	29	22.95	14.30	10.55
Averaging time	$1350\delta/U_b$	$960\delta/U_b$		$1200\delta/U_b$	

The results presented here were obtained for $Re = 5500$. The time interval (T) over which the results were averaged was taken as 75 multiples of a typical large-eddy turn-over time i.e. $T = 75L/U_b$. The predicted mean velocity and the Reynolds-stress components (presented as the root-mean-square fluctuations) are shown in Fig. 2. Also plotted there are results from previous LES and DNS studies. There is little that distinguishes the present results from the others obtained by LES, or indeed from the results of the DNS except, perhaps, close to the pipe axis where the DNS results for the radial fluctuations show an uneven and more rapid approach to the axis of symmetry condition. Our experience suggests that such behavior is sometimes due to the time period for averaging not being sufficiently long. The close correspondence elsewhere suggests that the grid resolution in this and in the other LES studies is such that the effects of the sub-grid-scale model are negligible.

Calculations of the thermal field in the stationary pipe were performed for two different boundary conditions viz. a constant wall temperature (Th1) and a constant heat flux (Th2). For the former, the wall temperature was fixed at 343.15 K and the bulk temperature at 293.15 K. The calculated temperature at the outlet was mapped back to the inlet where it was re-scaled to maintain the same bulk temperature. For the latter, the wall heat flux was set equal to 25 W/m^2 yielding a radial temperature gradient at the wall of 975.76 K/m. With this gradient fixed, the computations were performed using the cyclic thermal boundary conditions explained above. The predicted values of Nusselt number obtained using both boundary conditions are presented in Table 2, together with values obtained with DNS for the same Reynolds number. Also presented there is the value obtained from the experimental correlations of Gnielinski [28]. The DNS of Piller [30] were performed with the constant wall temperature boundary condition and the value of $Nu = 18.54$ correlates very well with the present value of 18.70 obtained with the same condition. In contrast, in the DNS of Redjem-Saad et al. [8], a constant wall heat flux boundary condition was used and here their higher value of $Nu = 19.36$ compares well with the present result of 19.33. The differences in the results obtained with the two types of thermal boundary conditions is most likely due to small differences that arise from

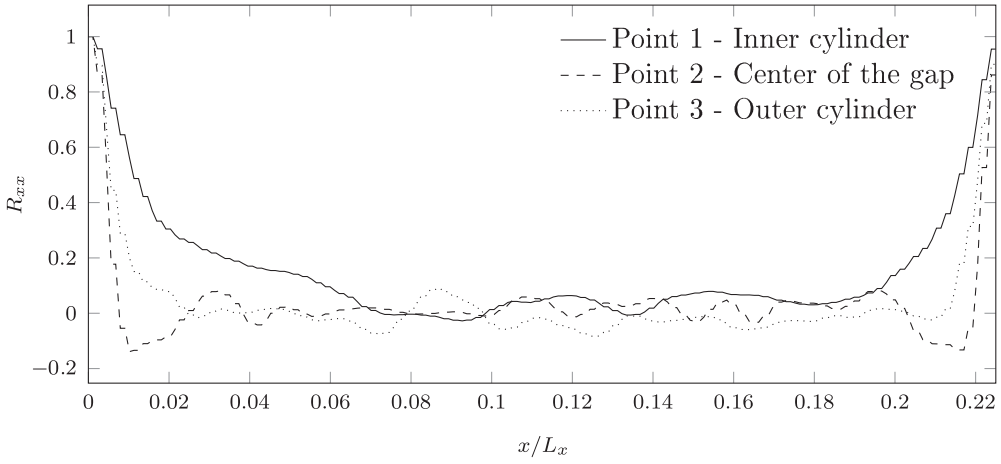

Fig. 6. Annular flow: Axial velocity two-point correlations coefficient.

calculating rather than prescribing the temperature gradient at the wall.

The predicted mean temperature, its variance, and the heat-flux components in the axial and radial directions are presented in Fig. 3. It is generally accepted that, similar to the case for velocity, the temperature, plotted in wall coordinates, varies linearly with distance from the wall within the viscous sub-layer, and logarithmically with the same distance in the fully turbulent region of the flow [31], thus:

$$\Theta^+ = Pr\ y^+$$

$$\Theta^+ = \frac{1}{\kappa_\theta}\ ln(y^+) + B_\theta \tag{11}$$

The DNS results of Satake [27] suggest the values $\kappa_\theta = 0.35$ and $B_\theta = 2.347$. These yield distributions that very closely match the present results. There is also much agreement between the various DNS and LES results for the temperature variance and the heat fluxes. It is interesting to note that while the axial gradients of temperature are far smaller than those in the radial direction, the axial heat flux ($\overline{u_x^+\theta^+}$) is almost one order of magnitude greater than the radial flux ($\overline{u_r^+\theta^+}$). This behavior can not be captured by a simple gradient-transport model such as Fourier's law since in such a model, the ratios of the fluxes would be proportional to the ratio of the temperature gradients in their respective directions.

Consideration is turned next to the case where the pipe is rotating around its longitudinal axis. With the angular velocity increasing in the radial direction away from the pipe axis, the sense of rotation is stabilizing the flow and the turbulence activity is expected to reduce relative to the stationary case. This is amply demonstrated in Fig. 4. Plotted there are the predicted radial profiles of the mean velocity and the Reynolds-stress components for two values of the rotation number, viz. N = 0.5 and 1.0. Also plotted there are the distributions for N = 0, and the experimental results of [5] and the DNS results [27] for the same rotation numbers. While the LES and DNS are generally in close correspondence with each other, some differences with the experimental results are apparent. These are due in part to the possibility that, in the latter, the flow had not yet reached a fully-developed state as evidenced by the departure of the measured shear stress $\overline{u_x^+ u_r^+}$ from the expected linear distribution. Both the LES and DNS show a steady reduction in the shear stress magnitude with increasing N. Similar trends are observed in the root-mean-square velocity fluctuations where the magnitudes of the near-wall peaks are reduced and displaced towards the pipe axis.

The predicted profiles of mean temperature, the temperature variance, and the turbulent heat fluxes are presented in Fig. 5. Profiles for N = 0 and 0.5 are presented, together with the DNS results

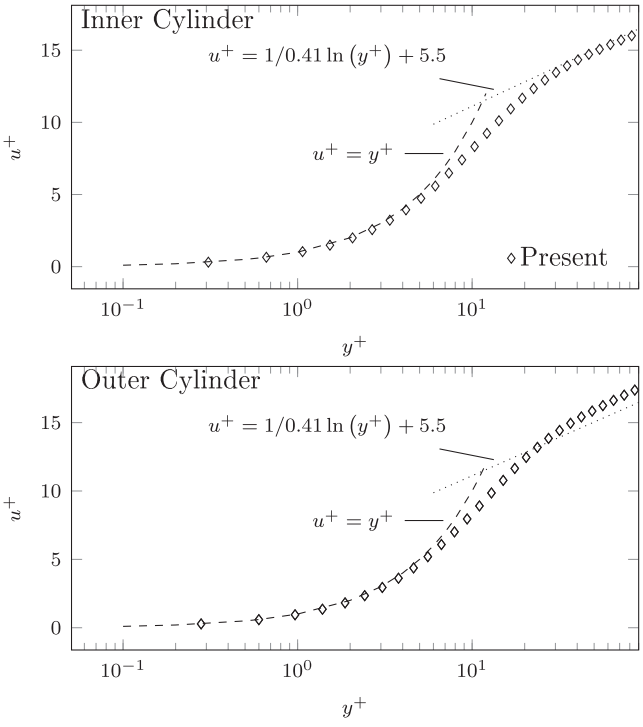

Fig. 7. Near wall velocity profile in wall units for inner and outer cylinder.

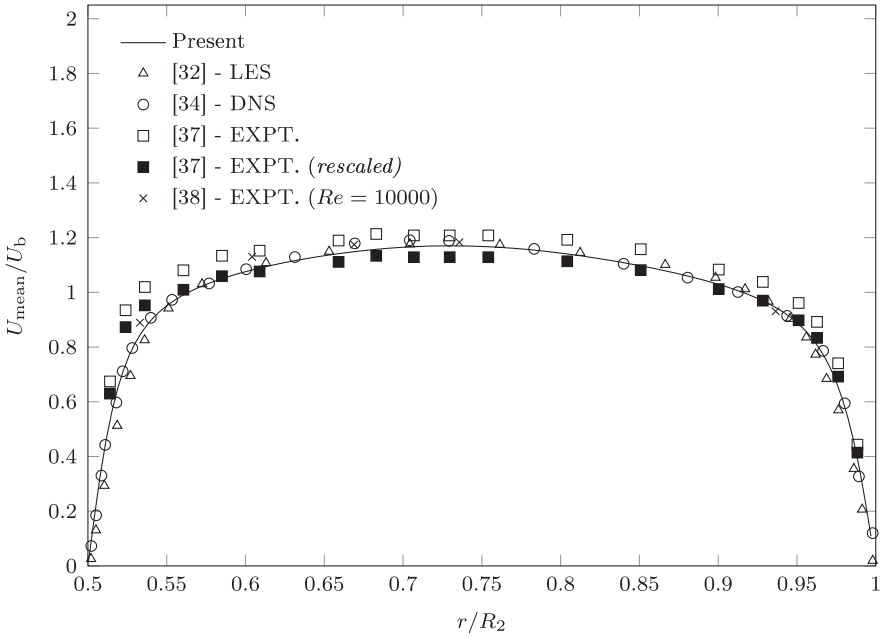

Fig. 8. Annular flow: Profiles of mean axial velocity. (See above-mentioned references for further information.)

Table 4
Mean flow parameters.

Researcher	Present LES	[34] DNS	[35] LES	[32] LES
Re	9000	8900	8900	8900
C_f (inner)	0.00961	0.00941	0.00981	–
C_f (outer)	0.00788	0.00848	0.00824	–
C_f (averaged)	0.00846	0.00880	0.00855	–
Re_τ (inner)	164.60	153.00	150.72	–
Re_τ (outer)	149.56	144.00	142.79	–
U_{mean}/u_τ (inner)	14.420	14.65	–	14.92
U_{mean}/u_τ (outer)	15.920	15.43	–	16.95

of [27]. The presence of rotation appears to produce opposite effects on the heat-flux components in the axial and radial directions, enhancing the former, but reducing the latter with respect to the stationary case. As before, the axial component is almost one order of magnitude greater than the radial component.

3.2. Annular flow

Here again our interest is confined to the fully-developed flow case in order to compare the present predictions with existing experimental data and with other numerical simulations. In what follows, the radius ratio R^* $(= R_1/R_2)$ was 0.5, and the Reynolds number (based on bulk velocity and hydraulic diameter) was set equal to 9000. The parameters that define the computational grid used here are given in Table 3 (with δ there being half of the annular gap width i.e. $1/2(R_2 - R_1)$).

In common with the other LES studies on annular pipe flows, the domain length L was taken as 2.25 D (≈ 18δ). To check that this length is sufficient to allow for the flow to become fully developed, two-point correlations for the fluctuating velocities were evaluated, thus:

$$R_{ii}(x_1, x_2) = \frac{\overline{u(x_1,t)u(x_2,t)}}{\sqrt{\overline{u_i^2(x_1,t)}}\sqrt{\overline{u_i^2(x_2,t)}}} \tag{12}$$

These correlations were evaluated for all three components of the fluctuating velocity, and at three radial locations viz. at the computational nodes closest to the surfaces of the inner and outer pipes, and at the node in the middle of the gap between them. In all cases, the correlations were evaluated with respect to conditions at inlet i.e. for $x_1 = 0$. The expectation was that the value of these correlations will, by definition, be unity at inlet, dropping thereafter to almost zero with increasing distance from inlet and then rising to become unity at the outlet plane consistent with the fact that the imposition of cyclic boundary conditions requires the conditions at the inlet and outlet planes to be perfectly correlated. This was indeed borne out in the present calculations, as can be seen from Fig. 6 where, for brevity, only the correlations for the streamwise component of velocity fluctuations (R_{xx}) are presented. As expected, the unity values at the inlet and outlet planes are

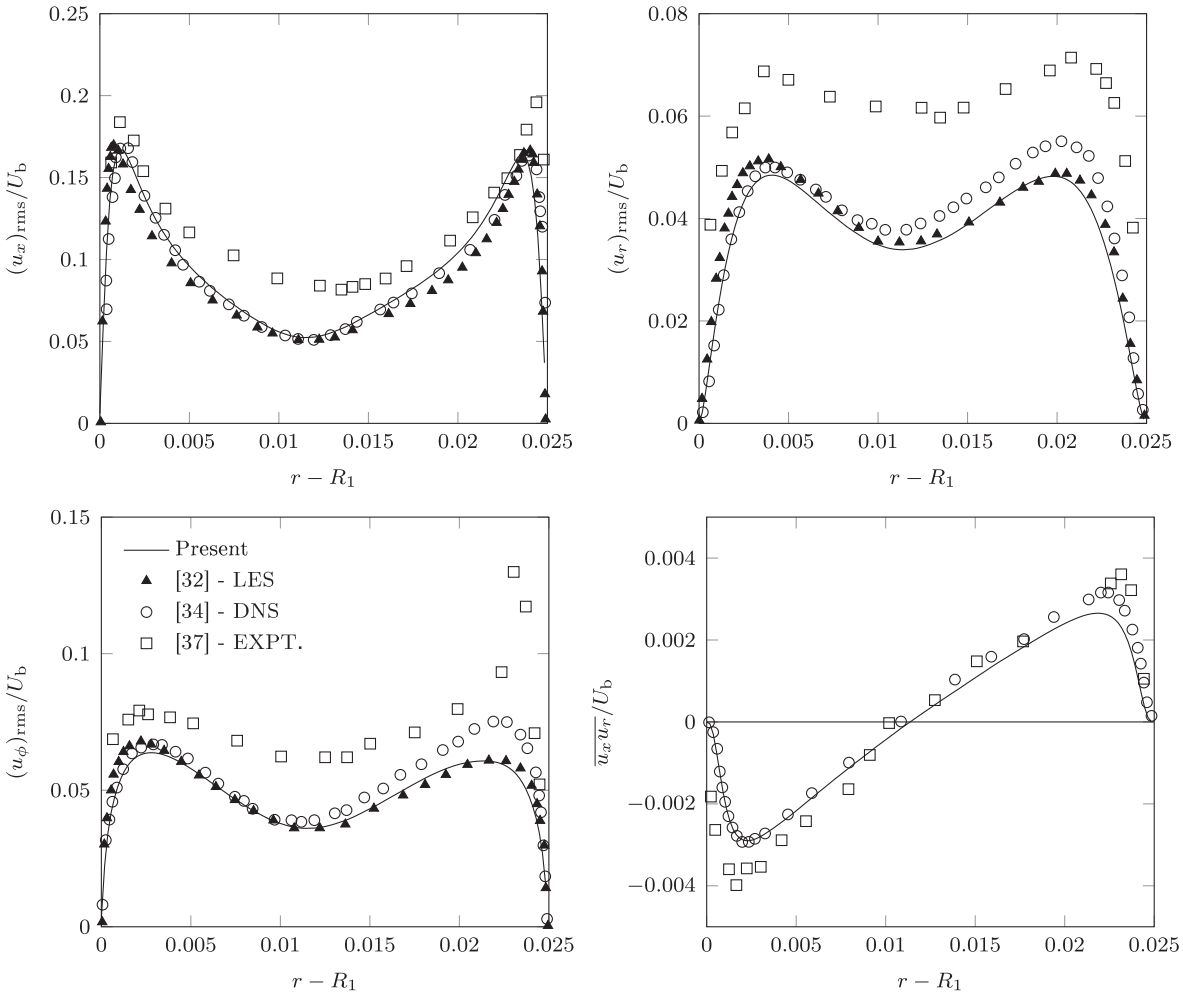

Fig. 9. Annular flow: Mean velocity and turbulence statistics.

obtained, together with the rapid drop to values around zero at a distance of around 1 D from the inlet. The drop to values of nearly zero in the two other correlations (R_{yy} and R_{zz}) was even more rapid than in R_{xx}, the latter being more susceptible to the presence of strong low-speed streaks [36].

For the case of annular flow with no rotation, the predicted mean velocity profiles are presented in Fig. 7. The profiles are plotted in wall coordinates using the appropriate values of friction velocity for the inner and outer walls. Also plotted there are the laminar-flow relation, and the log-law with the standard constants. The plots show that the computational grid provides for an adequate resolution of the viscous sub-layer with the grid nodes nearest to the walls being located at $y^+ < 1.0$, and with there being around 10 nodes within the range where $y^+ < 5.0$. In the outer regions of the flow, the log-law with standard constants appears to provide a good fit for the velocity near the inner cylinder but closer to the outer cylinder, the simulations appear to suggest that the log-region is better fitted with a lower values of both κ and B.

The predicted mean velocity profile, non-dimensionalized by the bulk velocity, is plotted in Fig. 8 where it is compared with available experimental data, and with results from LES and DNS. The experimental data of Nouri [37] were re-scaled as suggested by Chung [34] in order for the velocity profiles, when integrated across the annular gap, to yield a value that equals the quoted bulk velocity. The present predictions are in many places indistinguishable from other LES and the DNS results. Note the asymmetry in the mean-velocity profile with the maximum value occurring inboard of the mid-point of the annular gap.

The predicted skin friction coefficients for the inner and outer walls are presented in Table 4 where they are compared with other LES and DNS results. For the inner wall, the present results are close to the average of the previous computations while, for the outer wall, a lower value compared to the DNS result is obtained.

The cross-stream distributions of the Reynolds-stress components are presented in Fig. 9 where they are compared with measurements and with other simulations. While all the numerical simulations yield very similar distributions, especially for the root-mean-squares of the velocity fluctuations, the experimental data show consistently higher values everywhere in the gap.The asymmetry noted earlier in the mean velocity profiles is also present in the turbulent shear stress which changes sign at a point inboard of the gap center. This is well predicted in the present simulations.

Turning now to the heated annular flow, since the outer cylinder was adiabatic, the behavior of interest is confined to the vicinity of the inner wall which is where the following profiles are presented. In Fig. 10, these profiles are plotted in wall coordinates, and are compared with results from a number of previous direct numerical simulations. The differences between the various simulations are now somewhat more apparent and are most likely due to the differences in the time period over which the averaging of the instantaneous temperature fluctuations was performed. In

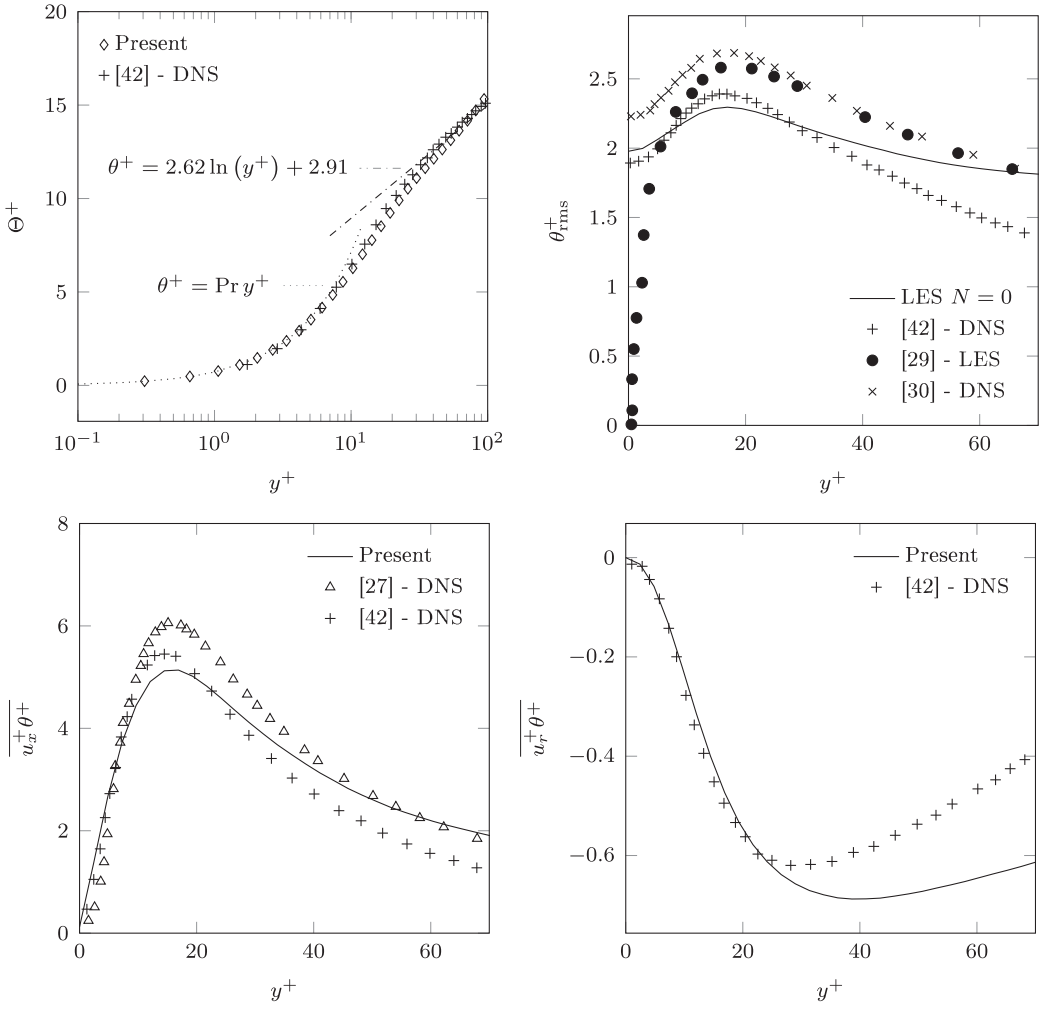

Fig. 10. Annular flow: Mean temperature and thermal statistics. (See above-mentioned references for further information.)

our experience, the averaging period required for the temperature fluctuating is always greater than that required for the velocity fluctuations.

The predicted Nusselt number is compared to the measurements of [40,41] in Table 5. The measured values are underestimated by about 5% due, in part, to the higher Reynolds number of Re = 10,000 used in these experiments.

Computations of the flow with rotating inner cylinder were performed for two rotation numbers, viz. N = 0.2145 and 0.858. These values were chosen to correspond to the values obtained in the experiments of [43]. The strength of rotation can also be quantified in terms of the Taylor number, defined as [34]:

$$Ta = \left(\frac{R_2 - R_1}{R_1}\right)^{0.5} U_{\Phi,wall}\frac{(R_2 - R_1)}{\nu} \tag{13}$$

The two rotation numbers considered here thus correspond to values of Ta of 1018 and 4075, respectively.

The predicted profiles of axial velocity for all three values of N are presented in wall coordinates in Fig. 11. The effects of destabilizing rotation are manifested in these plots by the apparent departures from the standard log-law, especially in the vicinity of the rotating inner wall, and at high rotation number. The effects of rotation propagate through the gap and are thus also felt in the vicinity of the outer wall albeit to a much lesser extent. The changes in the velocity profiles plotted in wall coordinates are directly attributable to the increase in the wall shear stress wrought by destabilizing rotation. This is clearly seen in Table 6 where the predicted skin friction coefficients for the inner and outer cylinders are presented for various rotation numbers. For the outer cylinder, the increase in C_f relative to the stationary case produce by the highest N amounts to about 50%, whereas for the inner cylinder, the corresponding increase is 84%.

The effects of destabilizing rotation on the root-mean-square values of the velocity fluctuations in the three coordinate directions are shown in Fig. 12. The greatest effect is seen in the radial velocity fluctuations u_r which is due to the increase in the rate of production of this quantity produced by the gradients of the circumferential velocity. Also affected, albeit to a lesser extent, is the tangential component of the velocity fluctuations u_ϕ - an effect which is due to the transfer of energy into this component by the

Table 5
Annular flow: Predicted and measured Nusselt number.

	Present LES	[39] ANA	[40] EXPT	[41] EXPT
Nu	25.64	26.34	27.07	27.08

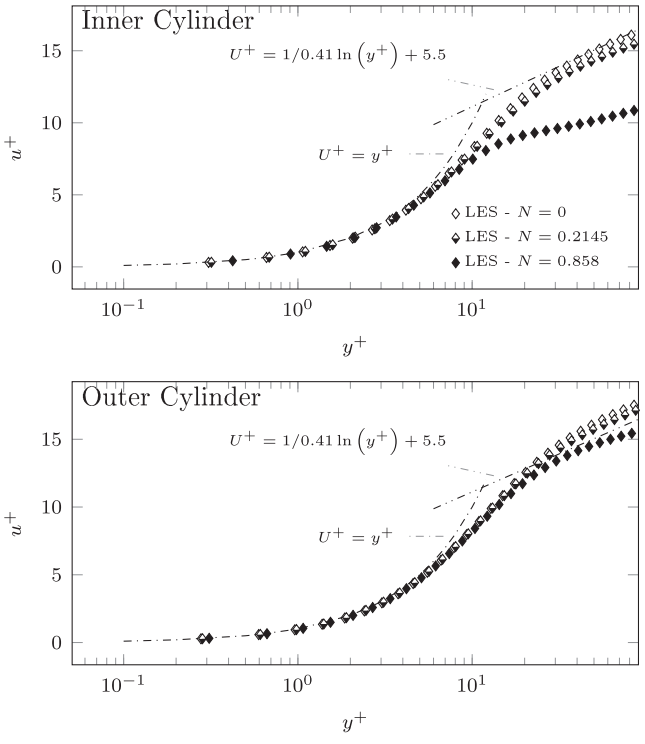

Fig. 11. Rotating annular flow: Mean velocity profiles near inner and outer walls.

Table 6
Annular flow: Skin friction coefficients for different rotation numbers.

	N	$C_{f_{outer}}$	$C_{f_{inner}}$	$C_{f_{averaged}}$
Present	0	0.0079	0.0095	0.0084
	0.2145	0.0081	0.0104	0.0088
	0.858	0.012	0.0175	0.0138
LES [33]	0.2145			0.00891
	0.429			0.00986
	0.858			0.0120
DNS [34]	0	0.00941	0.00848	0.00888

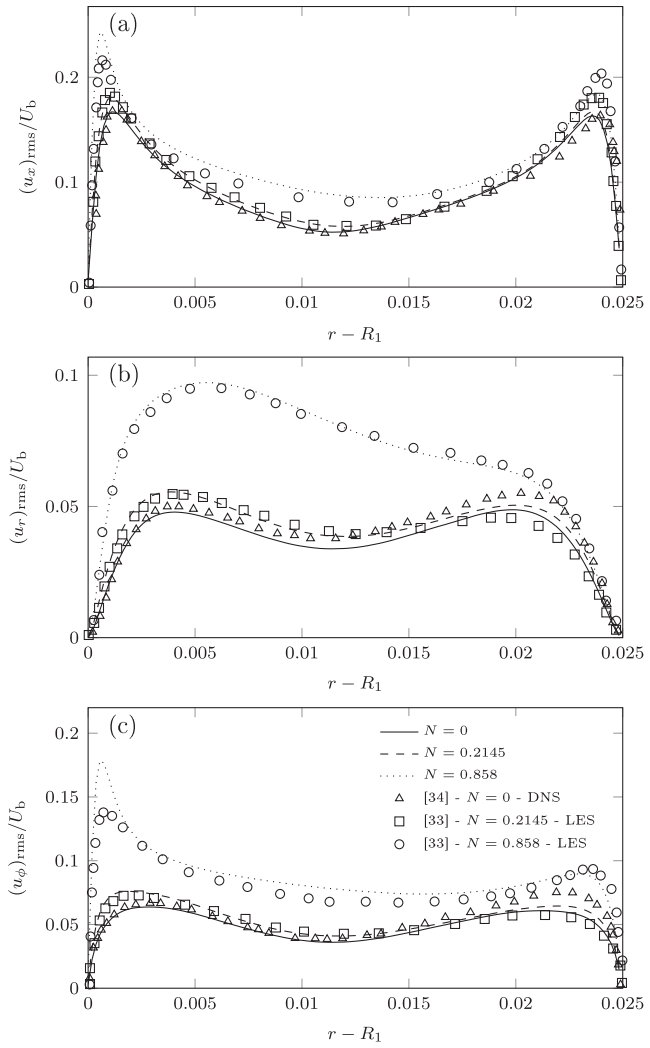

Fig. 12. Rotating annular flow: Root-mean-square of (a) axial, (b) radial and (c) azimuthal velocity fluctuations in wall units for $N = 0$, $N = 0.2145$ and $N = 0.858$.

action of the fluctuating pressure-strain correlations. The profiles of the axial component of fluctuating velocity become increasingly asymmetric with higher values of N where, here again, the rate of generation is enhanced by the radial gradient of tangential velocity.

The effects of rotation are also clearly evident in the profiles of the turbulent shear stress component $\overline{u_x u_r}$ which are shown in Fig. 13. Also plotted there are the LES results of [33] and the DNS results of [34]. As expected, the enhanced turbulence activity wrought by the inner cylinder rotation has led to significant increase in the level of this component relative to its value near the outer cylinder. Fig. 13 also shows the distribution of the two remaining components of turbulent shear stresses, namely $\overline{u_x u_\theta}$ and $\overline{u_r u_\theta}$. Note the change in sign of the first of these components - a behavior that is difficult to capture with Reynolds-stress transport closures. The sign of the other component is consistent with $\partial U_\theta/\partial r$ being negative throughout the annular gap.

It is of interest here to consider the implications of the above results on the computation of annular rotating flows using eddy-viscosity based turbulence closures. Such closures are usually based on Boussinesq's linear stress-strain relationship that aligns the Reynolds stresses with the appropriate mean rates of strain. In three-dimensional flows, this implies that the angle γ_g that mean strains make with the axial direction is coincident with γ_τ, the angle that the Reynolds stresses make with the same direction, where:

$$\gamma_g = \tan^{-1}\left[\frac{\partial \overline{U_\phi}/\partial r}{\partial \overline{U_x}/\partial r}\right], \gamma_\tau = \tan^{-1}\left[\frac{\overline{u_r u_\phi}}{\overline{u_r u_x}}\right]. \quad (14)$$

In Fig. 14, these angles are plotted against the radial distance. The behavior of γ_g follows from the fact that $\partial U_\Phi/\partial r$ is everywhere negative whereas $\partial U_x/\partial r$ is positive near the inner cylinder and negative near the outer one. For $N = 0.858$, the point where the mean-strain angle changes sign occurs at distance from the inner cylinder of approximately 0.24 δ. In contrast, the location where the shear-stress angle changes sign is located at distance of 0.28δ. Taken together, the results for $N = 0.21$ and 0.858 suggest that the misalignment between these angles increases very rapidly with N and this in turn suggests that eddy-viscosity closures would yield increasingly inaccurate predictions with increasing N.

The effects of destabilizing rotation on the thermal field are considered next. A sensitive indicator of the state of turbulence is the Nusselt number as its value is directly related to the strength of turbulent mixing in the near-wall region. Table 7 shows the variation of this parameter with N. Also presented in that table are the values suggested by the experimental correlations of [44]:

$$\frac{Nu}{Nu_0} = \left[1 + \left(\frac{2}{\pi}\frac{D_o}{D_i}\frac{U_{\phi,\text{wall}}}{U_b}\right)^2\right]^{0.8714} = \left[1 + \left(\frac{2}{\pi}\frac{1}{R^*}N\right)^2\right]^{0.8714}. \quad (15)$$

The present results, while adequately capturing the overall trend in the correlations, do not capture the rapid increase in Nu that occurs with increasing N. It is generally accepted that the increase in turbulence mixing due to destabilizing effects reaches a plateau which, in the present flow, would result in a slowdown in the rate at which Nu increases at higher values of N. In the absence of other LES or DNS results for the present value of R^*, the trends in Nu at higher rotation rates cannot be determined with much certainty.

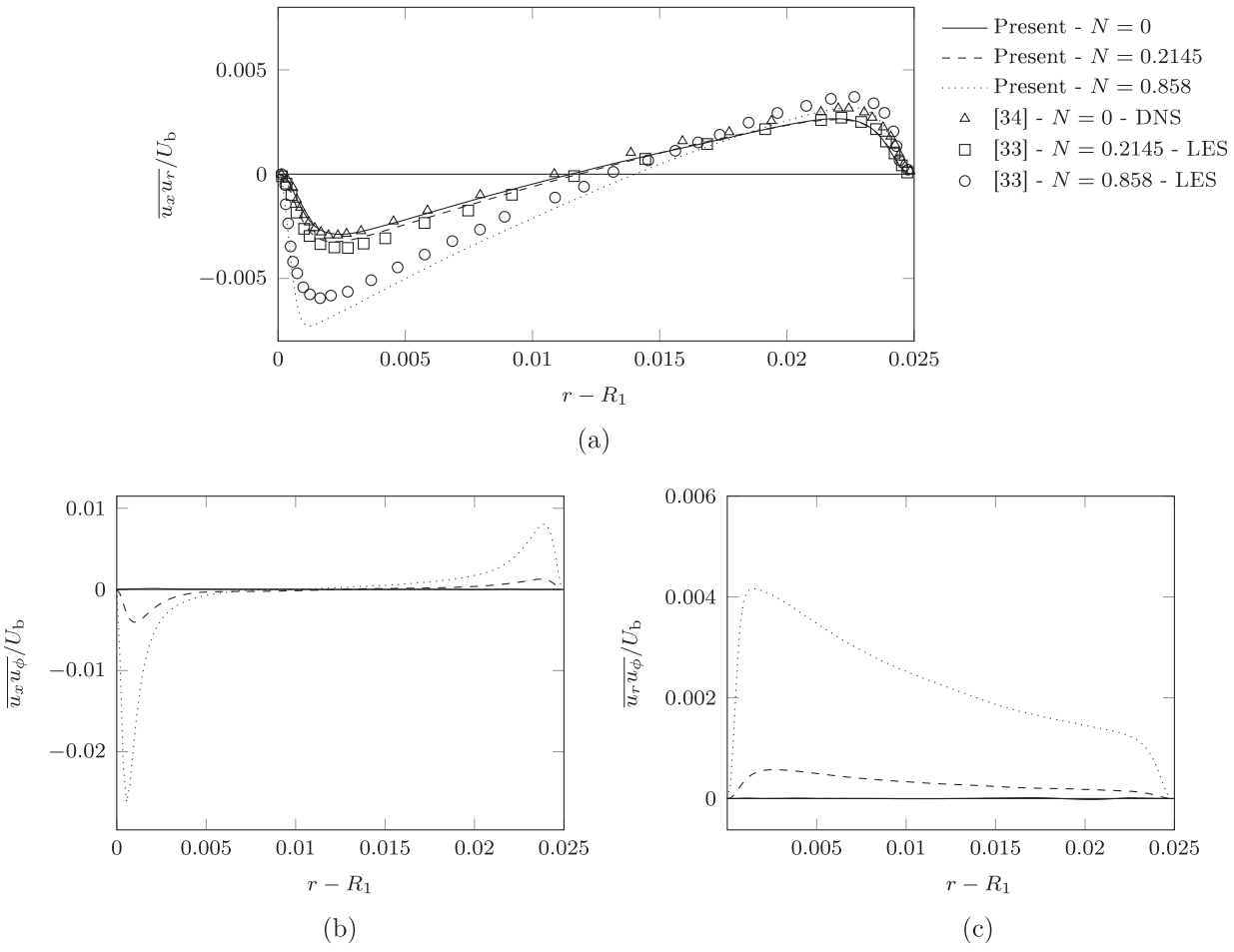

Fig. 13. Rotating annular flow: Distribution of Reynolds shear stress.

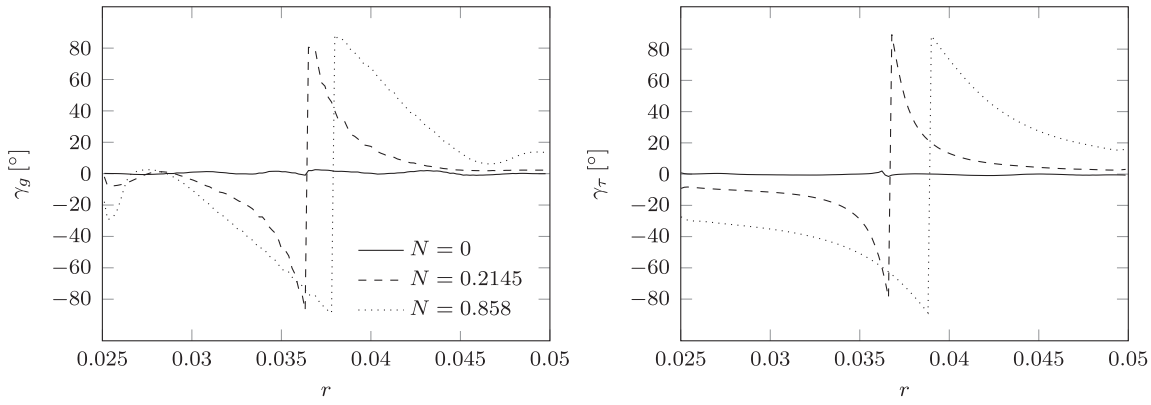

Fig. 14. Rotating annular flow: Direction of mean strain rate γ_g and Reynolds shear stress γ_τ.

Table 7
Nusselt number relation Nu/Nu_0 compared to experimental correlation.

	Present	[44]
N = 0	1.0	1.0
N = 0.2145	1.162	1.065
N = 0.858	1.856	1.982

The profiles of mean temperature, temperature variance and the heat-flux components are presented in Fig. 15 were all are non-dimensionalized with the friction velocity and friction temperature. The trends here are similar to those observed for the velocity field with the mean temperature distribution, for example, falling below the logarithmic distribution due to the substantial increase in the fluxes of both momentum and heat at the wall.

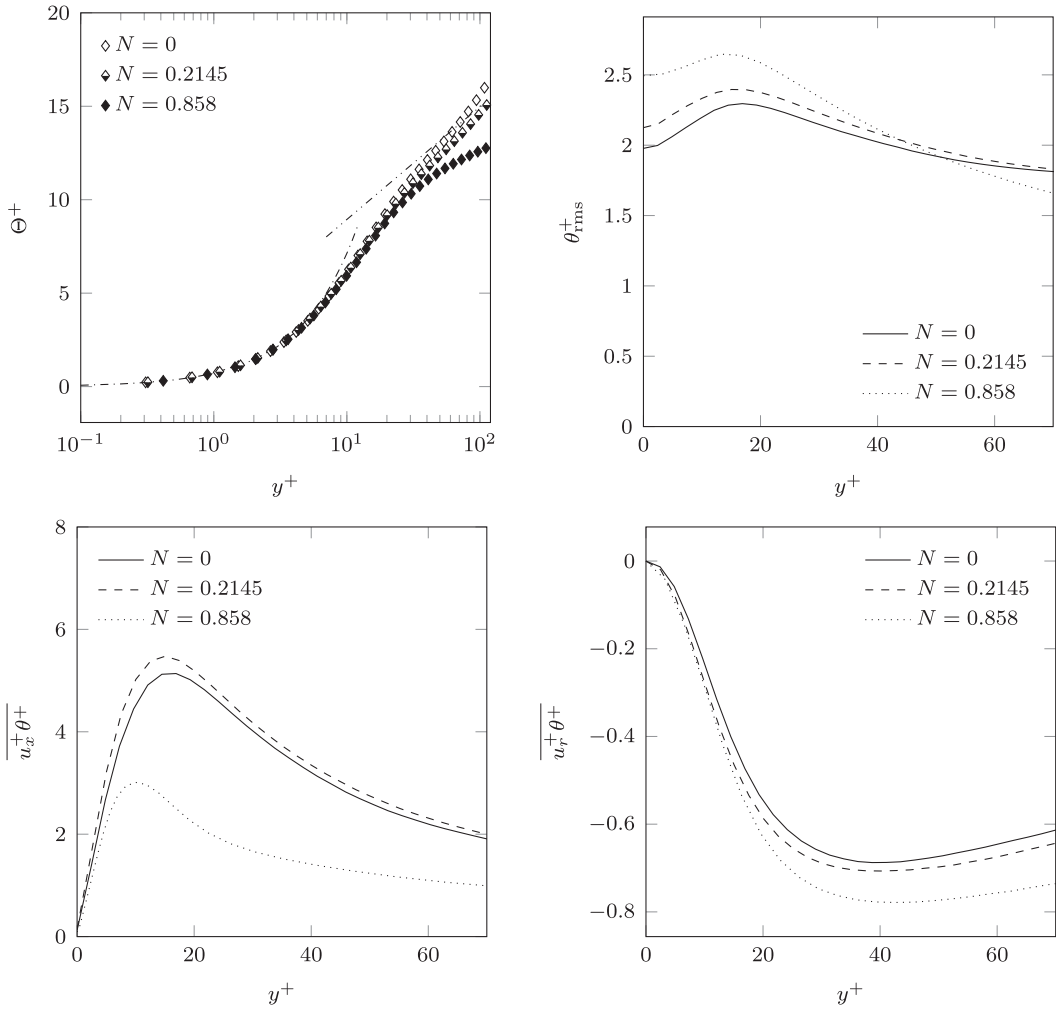

Fig. 15. Rotating annular flow: Mean temperature and thermal statistics.

4. Conclusions

Large eddy simulations of the heated flow in an annular gap with inner cylinder rotation were presented for two values of the rotation number ($N = 0.21$ and 0.858) and for $Re = 9000$. To better identify the effects of destabilizing rotation, comparative simulations were also performed for the stationary annular flow. The verification of the numerical solutions was accomplished via comparisons with previously published results from DNS, LES and experiments for the case of flow in a pipe with and without rotation. The destabilizing effects of rotation were most apparent in the vicinity of the inner cylinder where, at $N = 0.858$, the mean velocity profiles exhibited dramatic departure from the standard logarithmic law. This behavior suggests that engineering turbulence closures that rely on wall functions to bridge the viscous sub-layer will yield increasingly less accurate predictions with increasing N, especially for wall-related parameters such as the skin-friction coefficient and the Nusselt number. Another result that has implication for engineering turbulence closure is the asymmetry in the profile on mean axial velocity which becomes more prominent with increasing N. This asymmetry results in the displacement of the points where the velocity gradient and the Reynolds shear stress are zero. Eddy-viscosity closures that are based on Boussinesq's hypothesis assume that these points are always coincident, and hence such models will become unreliable with high values of N. The simulations also show that the direction of the resultant axial and tangential velocity gradients does not coincide with the direction of shear stress components in the same directions. This feature of rotating flows is entirely due to non-local effects arising from the transport of shear stress by combined mean-flow advection, and turbulent transport. In terms of turbulence closure, such mechanisms can only be captured by using complete Reynolds-stress transport models where the effects of mean-flow transport can be accounted for exactly, while those of turbulent transport would require the use of an appropriate model for the triple velocity correlations of turbulence.

Conflict of interest

The authors declared that there is no conflict of interest statement.

Acknowledgements

M. Schneider gratefully acknowledges the financial support provided by the Hermann-Reissner-Foundation and the Erich-Becker-Foundation that facilitated his stay at UC Davis.

Appendix A. Sub-grid scale model

The results presented above were obtained by setting the Smagorinsky coefficient $C_s = 0.065$. To check the sensitivity of the results to this value, calculations were performed with the sub-grid scale correlations obtained from Germano et al.'s [18] dynamic model, and again with no sub-grid scale model at all (i.e. with $C_s = 0$). The results, of which a representative sample is shown in Fig. A.16 where the turbulence kinetic energy k is plotted, indicate that the grid used was sufficient to render negligible the contributions of the sub-grid scale correlations to the flow field.

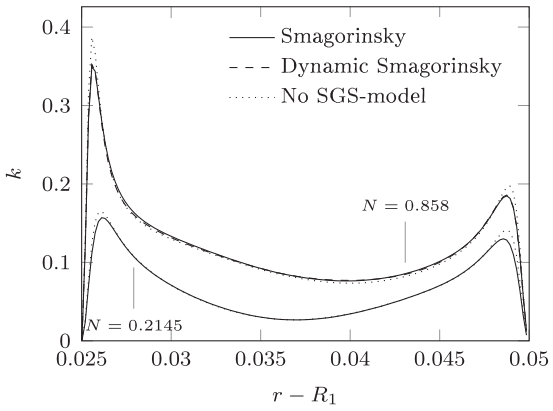

Fig. A.16. Turbulent kinetic energy.

References

[1] T.W.S. Rayleigh, On the dynamics of revolving fluids, Proc. Roy. Soc. 93A (1917) 148–154.
[2] K. Kikuyama, M. Murakami, K. Nishibore, K. Maeda, Flow in an axially rotating pipe: a calculation of flow in the saturated region, Bull. JSME 26 (1983) 505–513.
[3] B. Weigand, H. Beer, On the universality of the velocity profiles of a turbulent flow in an axially rotating pipe, Appl. Sci. Res. 52 (2) (1994) 115–132.
[4] A. White, Flow of a fluid in an axially rotating pipe, J. Mech. Eng. Sci. 6 (1) (1964) 47–52.
[5] G. Reich, H. Beer, Fluid flow and heat transfer in an axially rotating pipe—I. Effect of rotation on turbulent pipe flow, Int. J. Heat Mass Transfer 32 (3) (1989) 551–562.
[6] J. Eggels, J. Westerweel, F. Nieuwstadt, R. Adrian, Direct numerical simulation of turbulent pipe flow, Appl. Sci. Res. 51 (1–2) (1993) 319–324.
[7] S. Saha, C. Chin, Cheng, H. Blackburn, A. Ooi, Numerical study of heat transfer in a fully developed turbulent pipe flow, in: 17th Australasian Fluid Mechanics Conference. Auckland, New Zealand, 2010.
[8] L. Redjem-Saad, M. Ould-Rouiss, G. Lauriat, Direct numerical simulation of turbulent heat transfer in pipe flows: effect of Prandtl number, Int. J. Heat Fluid Flow 28 (5) (2007) 847–861.
[9] E. Tavakoli, R. Hosseini, M. Papalexandris, B. Lessani, Statistical analysis of instantaneous turbulent heat transfer in circular pipe flows, Heat Mass Transfer 50 (1) (2014) 125–137.
[10] M.R. Malin, B.A. Younis, The prediction of turbulent transport in an axially rotating pipe, Int. Commun. Heat Mass Transfer 24 (1) (1997) 89–98.
[11] C.G. Speziale, B.A. Younis, S.A. Berger, Analysis and modelling of turbulent flow in an axially rotating pipe, J. Fluid Mech. 407 (2000) 1–26.
[12] M. Fenot, Y. Bertin, E. Dorignac, G. Lalizel, A review of heat transfer between concentric rotating cylinders with and without axial flow, Int. J. Therm. Sci. 50 (2011) 1138–1155.
[13] K.M. Becker, J. Kaye, Measurements of diabatic flow in an annulus with an inner rotating cylinder, J. Heat Transfer 84 (2) (1962) 97–104.
[14] T.M. Kuzay, C.J. Scott, Turbulent heat transfer studies in annulus with inner cylinder rotation, J. Heat Transfer 99 (1) (1977) 12–19.
[15] A. Murata, K. Iwamoto, Heat and fluid flow in cylindrical and conical annular flow passages with through flow and inner wall rotation, Int. J. Heat Fluid Flow 32 (2011) 378–391.
[16] S.Y. Chung, H.J. Sung, Direct numerical simulation of turbulent concentric annular pipe flow: Part 2: Heat transfer, Int. J. Heat Fluid Flow 24 (3) (2003) 399–411.
[17] S.B. Pope, Turbulent Flows, Cambridge University Press, 2000.
[18] M. Germano, U. Piomelli, P. Moin, W.H. Cabot, A dynamic subgrid-scale eddy viscosity model, Phys. Fluids A 3 (7) (1991) 1760–1765.
[19] OpenFOAM. <www.openfoam.org>.
[20] S.V. Patankar, C.H. Liu, E.M. Sparrow, Fully developed flow and heat transfer in ducts having streamwise-periodic variations of cross-sectional area, ASME J. Heat Transfer 99 (2) (1977) 180–186.
[21] E. De Villiers, The Potential of Large Eddy Simulation for the Modelling of Wall Bounded Flows, PhD Thesis, Department of Mechanical Engineering, Imperial College – London, 2006.
[22] M. Ould-Rouiss, A. Dries, A. Mazouz, Numerical predictions of turbulent heat transfer for air flow in rotating pipe, Int. J. Heat Fluid Flow 31 (4) (2010) 507–517.
[23] M. Bousbai, M. Ould-Rouiss, A. Mazouz, A. Mataoui, Turbulent heat transfer characteristics of water flow in a rotating pipe, Heat Mass Transfer 49 (4) (2013) 469–484.
[24] Z. Yang, Large eddy simulation of fully developed turbulent flow in a rotating pipe, Int. J. Numer. Meth. Fluids 33 (5) (2000) 681–694.
[25] A.A. Feiz, M. Ould-Rouis, G. Lauriat, Large eddy simulation of turbulent flow in a rotating pipe, Int. J. Heat Fluid Flow 24 (3) (2003) 412–420.

[26] J. Eggels, F. Unger, M. Weiss, J. Westerweel, R. Adrian, R. Friedrich, F. Nieuwstadt, Fully developed turbulent pipe flow: a comparison between direct numerical simulation and experiment, J. Fluid Mech. 268 (1994) 175–210.
[27] S. Satake, T. Kunugi, Direct numerical simulation of turbulent heat transfer in an axially rotating pipe flow: Reynolds shear stress and scalar flux budgets, Int. J. Numer. Meth. Heat Fluid Flow 12 (8) (2002) 958–1008.
[28] V. Gnielinski, Neue Gleichungen für den Wärme-und den Stoffübergang in turbulent durchströmten Rohren und Kanälen, Forsch. Ing. A 41 (1) (1975) 8–16.
[29] M. Ould-Rouiss, M. Bousbai, A. Mazouz, Large eddy simulation of turbulent heat transfer in pipe flows with respect to Reynolds and Prandtl number effects, Acta Mech. 224 (5) (2013) 1133–1155.
[30] M. Piller, Direct numerical simulation of turbulent forced convection in a pipe, Int. J. Numer. Meth. Fluids 49 (6) (2005) 583–602.
[31] W. Kays, M. Crawford, B. Weigand, Convective Heat and Mass Transfer, fourth ed., McGraw-Hill, 2005.
[32] M. Hadžiabdić, K. Hanjalić, R. Mullyadzhanov, LES of turbulent flow in a concentric annulus with rotating outer wall, Int. J. Heat Fluid Flow 43 (2013) 74–84.
[33] S.Y. Chung, H.J. Sung, Large-eddy simulation of turbulent flow in a concentric annulus with rotation of an inner cylinder, Int. J. Heat Fluid Flow 26 (2) (2005) 191–203.
[34] S.Y. Chung, G.H. Rhee, H.J. Sung, Direct numerical simulation of turbulent concentric annular pipe flow: Part 1: Flow field, Int. J. Heat Fluid Flow 23 (4) (2002) 426–440.
[35] S.Y. Jung, H.J. Sung, Characterization of the three-dimensional turbulent boundary layer in a concentric annulus with a rotating inner cylinder, Phys. Fluids 18 (11) (2006) 115102.
[36] J.G.M. Eggels, Direct and Large Eddy Simulation of Turbulent Flow in a Cylindrical Pipe Geometry, TU Delft, Delft University of Technology, 1994.
[37] J.M. Nouri, J.H. Whitelaw, Flow of Newtonian and non-Newtonian fluids in a concentric annulus with rotation of the inner cylinder, ASME J. Fluids Eng. 116 (4) (1994) 821–827.
[38] S. Hirai, T. Takagi, K. Tanaka, T. Higashiya, Turbulent heat transfer to the flow in a concentric annulus with a rotating inner cylinder, in: 8th International Heat Transfer Conference, vol. 3, 1986, pp. 895–900.
[39] B. Weigand, M. Wolf, H. Beer, Heat transfer in laminar and turbulent flows in the thermal entrance region of concentric annuli: Axial heat conduction effects in the fluid, Heat Mass Transfer 33 (1–2) (1997) 67–80.
[40] J.S. Lewis, A heat-mass transfer analogy applied to fully developed turbulent flow in an annulus, J. Mech. Eng. Sci. 13 (4) (1971) 286–292.
[41] H. Pfitzer, H. Beer, Heat transfer in an annulus between independently rotating tubes with turbulent axial flow, Int. J. Heat Mass Transfer 35 (3) (1992) 623–633.
[42] S.Y. Chung, H.J. Sung, Direct numerical simulation of turbulent concentric annular pipe flow: Part 2: Heat transfer, Int. J. Heat Fluid Flow 24 (3) (2003) 399–411.
[43] J.M. Nouri, H. Umur, J.H. Whitelaw, Flow of Newtonian and non-Newtonian fluids in concentric and eccentric annuli, J. Fluid Mech. 253 (1993) 617–641.
[44] T. Kuzay, C. Scott, Turbulent heat transfer studies in annulus with inner cylinder rotation, J. Heat Transfer 99 (1) (1977) 12–19.